Dissecting the Role of Membrane Defects with Low-Energy Barrier on Fouling Development through A Collision Attachment-Monte Carlo Approach

Junxia Liu [1], Zhiwei Tang [1], Haiyan Yang [2], Xianhui Li [3,] *, Xuri Yu [1], Zhihong Wang [1], Tianyi Huang [1], Chuyang Y. Tang [4,] **

[1] School of Civil and Transportation Engineering, Guangdong University of Technology, Guangzhou 510006, China

[2] School of Environment, South China Normal University, Guangzhou, 510006, China

[3] Key Laboratory for City Cluster Environmental Safety and Green Development of the Ministry of Education, School of Ecology, Environment and Resources, Guangdong University of Technology, Guangzhou, 510006, P.R. China

[4] Department of Civil Engineering, The University of Hong Kong, Pokfulam, Hong Kong

Corresponding Author

* lixianhui@gdut.edu.cn (X. Li), ** tangc@hku.hk (C.Y. Tang)

Abstract

Membrane defects with low energy-barrier characteristics are unavoidable in membrane fabrication. However, their influences on fouling have not been fully understood. This work systematically investigates the critical role of membrane defects on fouling development and characteristics by adopting a collision attachment-Monte Carlo approach. Simulations show that membrane defects influencing on fouling is highly governed by foulant-clean-membrane interaction (F-M) and foulant-fouled-membrane interaction (F-F). When F-F energy barrier (E_f) is above a critical value (E_c), the long-term stability of water flux is not affected by the presence of defects, thanks to high F-F repulsion preventing further particles deposition. At low E_f ($<E_c$) but high F-M energy barrier E_m ($\geq E_c$), there appears an extended metastable flux for defect-free membrane. Since the local defects serve as hotspots to accelerate fouling, increased coverage or lowered energy barrier of defects shortens or even vanishes metastable period. For both low E_f ($<E_c$) and E_m ($<E_c$), severe fouling occurs at the beginning of filtration with/without defects as a result of the rapid fouling transition from F-M to F-F. Furthermore, membrane defects have less remarkable influences at higher initial flux where permeate drag plays a primary role. Our simulation provides important implications to membrane design and fouling mitigation.

Keywords

Membrane defects; Energy barrier; Foulant-clean-membrane interaction; Foulant-fouled-membrane interaction; Initial flux

1 Introduction

Membrane-based separation processes, such as reverse osmosis (RO) and nanofiltration (NF), play critical roles in desalination [1-3], water reclamation [4, 5], drinking water treatment [6, 7], and wastewater treatment [8, 9]. However, colloidal fouling consisting of inorganic colloidal particles and organic macromolecules remains one of the huge barriers in restricting their sustainable applications [1, 10]. The characteristics of colloidal fouling are strongly governed by the interplay of hydrodynamic conditions (*e.g.*, initial water flux or applied pressure) [11-13] and colloid-membrane interaction (which is further strongly affected by feed characteristics and membrane properties) [10, 14-17]. In general, higher operating flux induces much severer fouling due to the larger permeate drag acting on foulant [18, 19]. For charged colloids, mild fouling often appears at high pH value or low ionic strength as a result of the strengthened electrostatic repulsion of colloid-membrane or colloid-colloid [14, 16]. In parallel, membranes with more hydrophilic exhibit better anti-fouling performance compared to the hydrophobic membranes, thanks to the intensified hydrophilic repulsive interaction between colloids and membrane [20, 21].

Membrane defects, generally formed from the undesired membrane preparation process [1, 22], have significant influence on membrane separation performance [23-26]. In addition to impairing membrane permselectivity [25, 27], the defective regions of

membrane surface with local larger-size pores, more thin skins or valley-like structures are more subject to initial foulants deposition [23, 24, 26, 28]. As a typical example, Elimelech and co-workers demonstrated that membranes with rough surface were more susceptible to fouling than that with smooth surface, and the initial silica colloids were preferentially accumulated at the valleys of the rough membrane [28, 29]. They further attributed the high fouling potential of the valley-like regions to their low colloid-membrane repulsion [30]. However, insignificant difference in flux decline was also observed on RO membrane with different roughness during filtrating bovine serum albumin (BSA) solution in a recent publication [13]. These contradictory observations from the literatures inspire us to dissect the role of membrane defects (*i.e.*, local regions of low energy barrier) on fouling characteristics.

In view of the variety of colloidal foulants, *e.g.*, silica colloid, humic acid, protein, etc. in raw water[10], the inconsistent observations in previous publications may be reconciled by considering the various foulant-foulant interaction. Although the initial fouling is dominated by foulant-clean-membrane interaction (F-M), the fouling will transit into being dominated by foulant-fouled membrane interaction (*i.e.*, foulant-deposited foulant interaction, F-F) once the membrane surface is completely covered by foulants [10, 15]. Presumably, at low F-F energy barrier (E_f), these preferential deposited foulants on the defective regions may serve as hotspots, favoring for more coming particle deposition owing to the weak F-F repulsion, in which the existence of

81 defects (or valley-like regions) might accelerate fouling development. While at high E_f,
82 the initial particles attached on the defective (or valley-like) regions might result in a
83 strong F-F repulsion, retarding further foulant deposition. As a result, these defects
84 might be repaired by the initial attached foulants and thus have no significant influence
85 on fouling. Furthermore, the effect of membrane defects is also expected to be highly
86 affected by initial flux since greater water flux can lead to a more hydrodynamic drag
87 to accelerate fouling transition from F-M to F-F [15]. All these uncertainties need to be
88 carefully examined to gain a better insight into the role of defects on membrane
89 performances.
90
91 Herein, we employ a stochastic collision attachment (CA)-Monte Carlo (MC) model
92 [15] to systematically investigate the influences of defects of RO/NF membranes on
93 fouling development and characteristics. In the CA-MC simulation, the development of
94 membrane fouling is treated as transport and collision of foulant particles towards the
95 membrane, and their subsequent attachment onto the membrane. More importantly, the
96 CA theory can scale the role of colloid-surface interaction as well as the hydrodynamic
97 interaction on fouling [19], while the MC simulation is able to simulate local fine details
98 of particles transport and attachment at the hydrodynamic boundary layer [15]. The
99 coupled CA-MC simulation will therefore deeply disclose the critical role of the local
100 defects (*i.e.*, the existence of low energy barrier regions) of membrane surface on
101 fouling development and characteristics under different colloid-surface interactions as

well as operating flux. Simulations can reconcile the contradictory experimental phenomena of the defects influencing on fouling. Our findings also provide new insights and important implications for fouling mitigation.

2 Theory

The classical CA theory is originated from the field of coagulation, where it has been widely used to simulate the particle-particle collision and attachment [31]. Recently, Liu and co-workers [19] brought it into membrane filtration process, realizing a membrane as a large particle, and fouling as a series of particles transport and collision with the membrane, followed by their attachment onto the membrane. Based on CA theory [16, 19], the rate of particle deposition is determined by the collision frequency of colloidal foulants and the probability of successful colloidal attachment (*i.e.*, attachment coefficient α). In particular, α is strongly dependent on hydrodynamic interaction and colloidal-membrane interaction [19], and its value can be scaled by the Boltzmann distribution [32]. To dissect the fouling behavior shifting from F-M to F-F interaction, Liu et al. [15] further adopted a stochastic CA-MC approach to simulate the random processes of colloidal transport and attachment in the fouling formation and development.

2.1. Problem setting up

To simulate the role of local defects on fouling development and characteristics, a two-dimensional (2D) membrane channel model, with length L and height δ (*i.e.*, boundary layer thickness), is established (Figure 1). Similar to our previous report [15], a cross flow with a constant velocity (u) continuously passes from left to right, and particles leaving the right boundary are returned back to the left boundary within their expected lifetime. At the same time, water also transports towards the membrane with a permeate flux of J under the constant applied pressure. To enable the simulation of local defects, the membrane along its length is equally divided into n grids, in which m ($0 < m \leq n$) segments are denoted as defects, in which the energy barrier of foulant-defective-segments interaction (F-D) (*i.e.*, energy barrier of defects, E_{md}) is less than that of foulant-defect-free-segments interaction (*i.e.*, E_m of F-M). It is worthy to note that the coverage of defects (*i.e.*, density of defects Φ_{md} ($=m/n$)) and the energy barrier of defects E_{md} are pre-programmed, while the locations of the defective segments are randomly generated. In the simulation, the CA-MC approach comprises following three steps: (1) particles transporting towards the membrane; (2) particles colliding with the membrane surface; and (3) particles attaching onto the membrane.

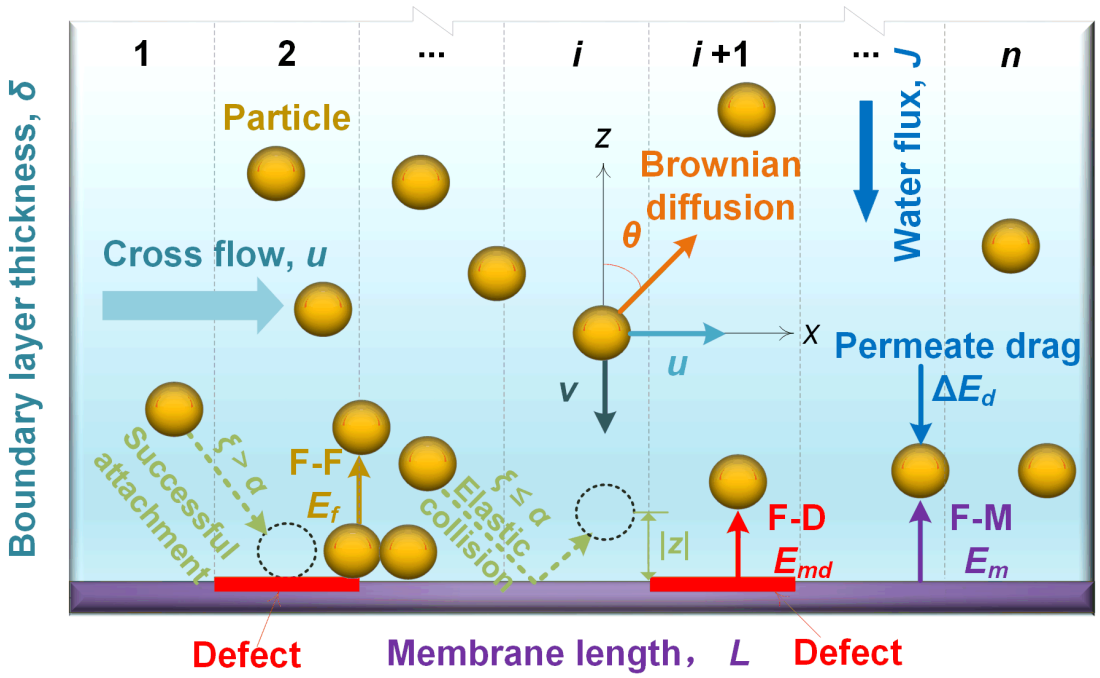

Figure 1. Schematics of membrane channel with colloidal transport and attachment

Since the NF and RO membranes are not designed to treat large-size foulants due to use of extensive pretreatments [33-35], this work only considers the effect of colloids with small size (d_p <100 nm), whose back migration is mainly governed by Brownian movement [10].While for large-size colloids (d_p > 100 nm), the additional influences of shear-induced diffusion and lateral migration (i.e., inertial lift force) need to be taken into account [36, 37]. We further assume a dilute foulant concentration. This assumption implies a relatively large average distance between colloids such that the foulant-foulant interaction in the solution can be negligible [10, 38]. Therefore, the aggregation of foulants in the boundary layer is not considered in this work.

2.2 Particle transport

As shown in Figure 1, colloidal transport in fluid channel is governed by the horizontal crossflow in x direction and the vertical permeate flow in -z direction, in addition to their self-diffusion with the random angle θ ranging from 0 to 2π. The displacement (*i.e.*, Δx and Δz) of a particle in each small interval (Δt) can be expressed as [15]:

$$\Delta x = u\Delta t + \sqrt{2 \times 2D\Delta t}\sin\theta \quad (1a)$$

$$\Delta z = -v\Delta t + \sqrt{2 \times 2D\Delta t}\cos\theta \quad (1b)$$

where u is the crossflow velocity, D is the Brownian diffusion coefficient, and v is the localized drag velocity. The value of D can be computed by the Stokes-Einstein equation [19], and the term $\sqrt{2\times 2D\Delta t}$ scales the distance of particle Brownian movement [39]. Furthermore, the value of v can be interpolated based on the localized permeate flux of two adjacent segments i and i +1 [15]:

$$v = (J_{i+1} - J_i)\frac{L_x}{L_e} + J_i \quad (2)$$

where J_i and J_{i+1} are the average flux at the grid i and i +1, respectively. L_e is the horizontal distance between the center lines of the two segments, and L_x is horizontal distance between the particle and the center line of segment i.

2.3 Particle collision

Due to the permeate drag, particle can move towards the membrane. Since the membrane is put at z value of zero, a collision event happens when particle's z value becomes negative. In this event, we use the attachment coefficient α (see the section 2.4 "Particle attachment") to account for the probability of the particle being successfully attached onto the membrane. As seen in Figure 1, a stochastic number ξ ranging from 0 to 1 is generated in each collision process. If $\xi \leq \alpha$, the particle is successfully attached onto membrane surface. If $\xi > \alpha$, the particle will still stay in the feed solution, where its new vertical location resets to $|z|$ by assuming an elastic collision [15].

2.4 Particle attachment

Colloidal attachment is governed by hydrodynamics and colloid-surface interaction [16, 19] (see Figure 1). The probability of successful foulant attachment (α) can be simulated by Boltzmann distribution law [19]:

$$\alpha = \frac{1}{1 + \exp\left(\frac{\Delta E_b - \Delta E_d}{k_B T}\right)} \quad (3)$$

where k_B and T represent the Boltzmann's constant and the solution temperature, respectively. ΔE_b is the energy barrier of foulant-membrane interaction in resisting

fouling [16]. The term ΔE_d ($=\beta J$) accounts for the role of permeate drag exerted on foulant in promoting fouling, where β and J are the drag interaction coefficient and water flux, respectively [19]. A high flux J can supply great drag to conquer the energy barrier ΔE_b, resulting in a large α, whereas a small α occurs at a high ΔE_b with strong repulsion in retarding particle deposition. Due to the lower energy barrier of F-D, a relative larger α is expected in defective segments compared to the defect-free segments.

When particles successfully attach onto the membrane during collision process, they will modify the local colloid-membrane interaction. For segments with defect-free, the energy barrier ΔE_b is shifted from E_m of F-M to E_f of F-F interaction [15]:

$$\Delta E_b = (1-\omega)E_m + \omega E_f \quad (4a)$$

For defective segments, the energy barrier is shifted from E_{md} of F-D to E_f of F-F interaction:

$$\Delta E_b = (1-\omega)E_{md} + \omega E_f \quad (4b)$$

where ω is a coefficient for weighting the effect of deposited foulant on energy barrier. The value of ω_i for any given segment i is dependent on its surface coverage, as well as the influences of the neighbor segments i -1 and i +1 [15]:

$$\omega_i = (s_c)_i + \varphi(s_c)_{i-1} + \varphi(s_c)_{i+1} \qquad 0 \le \omega_i \le 1 \qquad (4c)$$

where s_c is the coverage ratio of the number of deposited foulant particles N_a to the number of particles required to fully cover the segment N_c (*i.e.*, $s_c=N_a/N_c$). φ is a neighbor coefficient describing the function of particle deposition of the neighbor segments, with a value of 0.1 adopted in this simulation.

2.5 Permeate flux

The deposited particles can also affect the localized water flux. The water flux in any grid can be determined according to the permeate flux model [15, 40]:

$$J = \frac{\Delta P}{\mu\left(R_m + \alpha_N \times N_f\right)} \qquad (5)$$

where ΔP is the operating pressure, μ is the feed viscosity, α_N is specific cake resistance, and N_f is the number of deposited particles.

The above CA-MC approach can be used to model the coverage of defects Φ_{md} and energy barrier of defects E_{md} influencing on the behavior of water flux, particle transport and deposition during membrane filtration. The specific algorithm procedure is documented in Supporting Information S1.

3 Experimental validation

In our previous study for humic acid fouling, the predicted water flux by CA-MC model was in well agreement with the experimental results[15]. To further verify the accuracy of the fouling model established in current study, we herein compare the CA-MC simulations with the experimental data for protein fouling, in which a commercial nanofiltration membrane (NF270) is fouled by BSA over a series of applied pressure (25-140 psi) at respective solution pH of 7.0 and 5.8. It should be noted that the applied pressures and solution pHs can represent the influences of hydrodynamics drag and colloid-membrane interaction on fouling development, respectively [14, 16, 18, 19]. As shown in Figure 2a and 2b, the simulations (the dashed lines) agree well with the experimental data (the scattered dots). In general, membrane flux is more stable at lower operational pressure (or initial flux) owing to the decreased hydrodynamics drag, which corresponds to the theory of critical flux [10, 41]. For high operational pressure (*i.e.*, 110 – 140 psi), more severe fouling occurs at lowered solution pH (*i.e.*, from 7.0 to 5.8) as a result of the reduced energy barrier of foulant-membrane interaction (see Supporting information S2), which is consistent with the existing literatures on the effect of solution chemistry [11, 16]. Model validation suggests that our CA-MC approach is capable of correctly predicting not only the role of hydrodynamics but also the effect of colloid-membrane interaction on fouling.

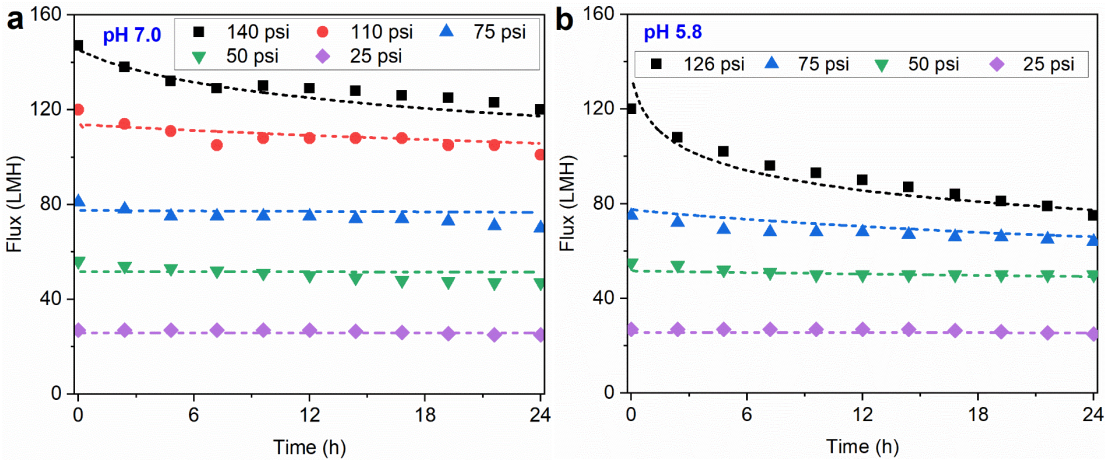

Figure 2. Model validation for BSA fouling of NF membrane. Water flux as a function of time at solution pH value of (a) 7.0 and (b) 5.8. The experimental data (the scattered dots) are obtained from our prior study[12], and the detailed experimental conditions were documented in Ref. [12]. The dashed lines represent the CA-MC simulation results, with the detailed simulation parameters for model validation listed in Supporting information S2.

4 Results and discussion

4.1 Water flux at different coverage of defects

The initial and long-term fouling are governed by E_m originating from F-M interaction and E_f arising from F-F interaction, respectively [15]. In real application, membranes are often designed with better antifouling ability, *i.e.*, high F-M repulsion, while the F-F interaction is always restricted by colloidal type and properties. To cater for the true situation, Figure 3 exhibits the effects of coverage of defects Φ_{md} (at E_{md} of 6 k_BT) on flux declines at the conditions of a relatively high E_m (12 k_BT) but low E_f (3 k_BT), with the main parameters used for modelling listed in Table 1. At a low initial flux of 10 μm/s, membrane defects have significant influences on fouling formation (Figure 3a). Specifically, no fouling is observed for the case of evenly perfect membrane without

272 defects (Φ_{md} = 0/50) during the whole filtration period, thanks to the strong F-M
273 repulsion of entire membrane surface. Increasing Φ_{md} from 1/50 to 10/50 leads to the
274 enhanced flux loss from about 4% to 25% at the whole 1000-min period owing to the
275 increased coverage of low energy barrier regions over membrane surface. Under the
276 most unfavorable condition Φ_{md} = 50/50, in which the clean membrane surface is
277 completely covered by defects resulting in lack of effective resistance against particle
278 deposition, the water flux at the end of 1000-min filtration decreases by more than 40%
279 of its initial value. Our simulations reveal the importance of minimizing the coverage
280 of membrane defects to avoid serious flux drops.

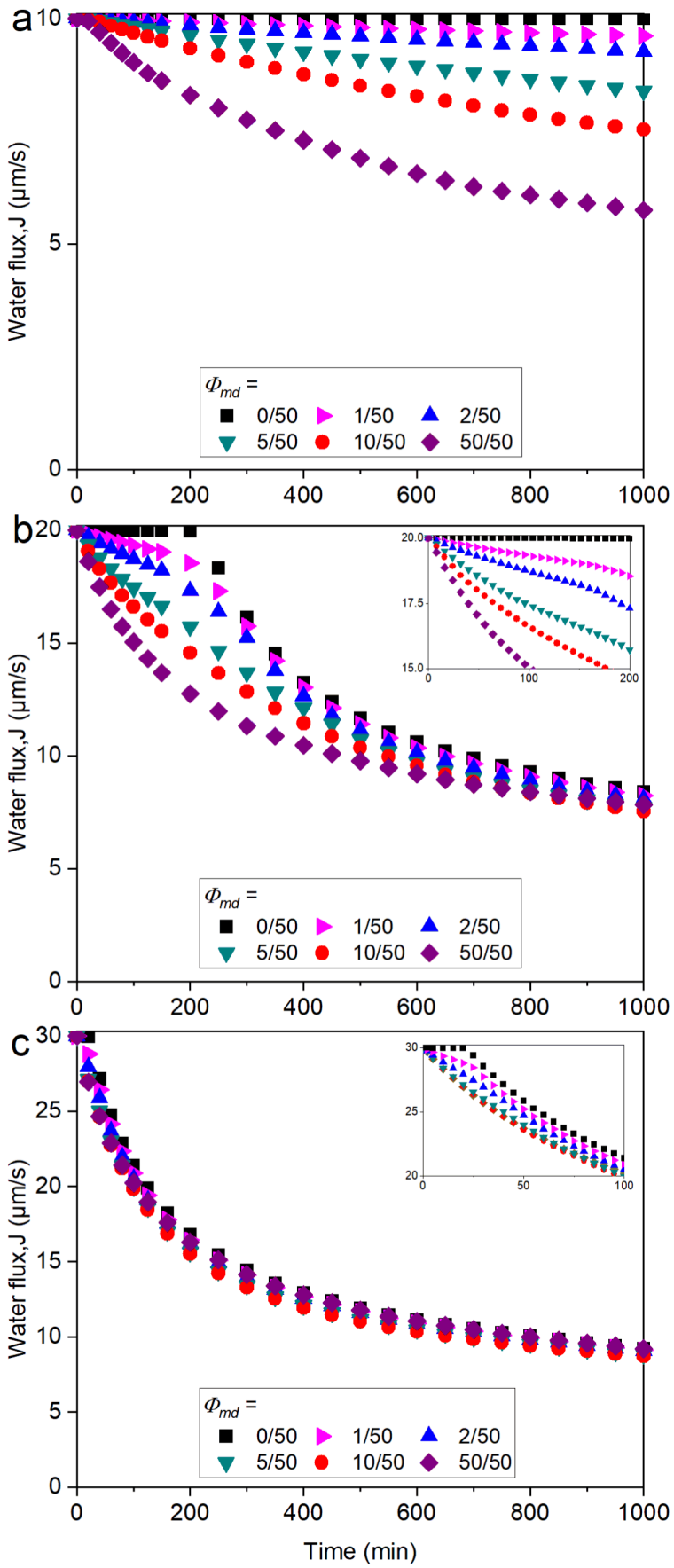

Figure 3. Effect of coverage of defects Φ_{md} on flux decline at (a) J_0= 10 μm/s; (b) J_0=

20 μm/s; and (c) J_0= 30 μm/s. Simulation conditions: Φ_{md}=0/50 – 50/50, E_m = 12k_BT, E_{md} =6 k_BT, E_f = 3 k_BT, and the other modelling conditions listed in Table 1. Five runs of random CA−MC simulations for Φ_{md}=5/50 are given in Supporting Information S3.

Table 1. Parameters used for CA-MC simulation

	[a]Parameters	Value	Remarks
Foulant properties	d_p	2.0 ×10^{-8} m	Ref. [19]
	ρ	1.5×10^6 g/m^3	Ref.[15]
	m_p	$\rho\pi d_p^3/6$	In g/#
Feed properties	T	298.15 K (25°C)	Ref. [18]
	μ	8.9 ×10^{-4} Pa.s	Ref. [18]
	C_b	5.0 g/m^3	Ref. [18]
	C_n	C_b/m_p	In #/m^3
Operation conditions	ΔP	0.4-1.2 MPa	See Note[b]
	u	0.2 m/s	Ref. [19]
	R_m	4.5×10^{13} m^{-1}	Ref. [19]
	α_N	3.0 × 10^{13} ×m_p	Ref.[15]
	J	$\Delta P/(R_m+\alpha_N \times N_f)$	Eq. 5
Brownian diffusion	k_B	1.38 ×10^{-23} J/K	
	D	$k_BT/3\pi\mu d_p$	Ref. [42]
Interaction energy	k_BT	4.11×10^{-21} J	
	ΔE_b	0-12 k_BT	
	β	4.19×10^{-9} × d_p	Ref. [19]
Boundary layer	δ	5.0 ×10^{-6} m	Ref. [18, 19]
	L	5.0 ×10^{-5} m	Ref.[15]
	L_e	1.0 ×10^{-6} m	Ref.[15]
Simulation time	Δt	5.0 ×10^{-3} s	Ref.[15]
	t_{max}	$D\times(\exp(\delta J/D)-1)/J^2$	Ref.[15]

Note: [a]Particle size (d_p), Particle density(ρ), Particle mass (m_p), Temperature (T), Solution viscosity (μ), Particle mass concentration (C_b), Particle number concentration (C_n), Operational pressure (ΔP), Crossflow velocity (u), Membrane inherent resistance (R_m), Specific cake resistance (α_N), Water flux (J), Boltzmann's constant (k_B), Brownian Diffusion coefficient (D), Unit energy (k_BT), Energy barrier (ΔE_b), Drag energy coefficient (β), Boundary thickness (δ), Boundary length (L), Length of each region (L_e), Time step (Δt), Maximum particle lifetime (t_{max}). [b]This pressure range corresponds to permeate water flux ranging from 10 to 30 μm/s (i.e., 36 – 108 L/m^2.h), which covers the typical water flux used in RO and NF operations.

297 A severer fouling occurs at medium J_0 of 20 μm/s (Figure 3b). At a 1000-min filtration
298 period, all the flux curves collapse to nearly identical low value (< 50% of J_0). The
299 crucial role of water flux on fouling has been reported in previous studies: increased
300 initial flux exerts larger permeate drag, accelerating particle transport and attachment
301 [15, 16, 19]. Furthermore, our simulation is also consistent with the existing reports:
302 the long-period fouling is largely dependent on F-F interaction once the membrane
303 surface is fully covered by foulant particles [10, 18]. Despite that, our results clearly
304 indicate that the initial flux behavior is highly affected by the coverage of local defects.
305 At Φ_{md} = 0/50, water flux curve can maintain approx. 220-min stability before
306 appearance of a substaintial decline. Such phenonmenon on metastable flux was also
307 obseved in prevous litertures [12, 20, 43], whose period strongly depended on F-M
308 interaction [15]. With the increase of the Φ_{md}, an obvious decline of flux is observed at
309 the initial 200 min even with only 1/50-2/50 of membrane segments endowed with
310 defects. Further increasing Φ_{md} to ≥ 5/50 leads to rapid flux declines at the beginning
311 of filtration.
312
313 When the initial flux further increases to a relatively high value of 30 μm/s, the effect
314 of membrane defects on flux is less discernible except at the initial 20 min (Figure 3c).
315 While the energy barrier of colloid-membrane interaction plays a critical role in low
316 and medium fluxes of 10 – 20 μm/s (Figure 3a, b), the hydrodynamic drag becomes the
317 predominant effect at high J_0 of 30 μm/s (Figure 3c). Indeed, an increased permeate

318 drag will simultaneously increase colloidal transport velocity (Eq. 2) and the probability
319 of successful colloidal attachment (Eq. 3), hence greatly destabilizing the particles and
320 making them to easily deposit onto the membrane. Our results are in well agreement
321 with the recent literatures that membranes with larger initial flux suffered from severe
322 fouling regardless of the differences in their surface roughness [13] and colloid-
323 membrane interaction [44]. In view of much significant fouling trend at great permeate
324 flux, blindly elevating operating flux should be strictly prohibited in large-scale
325 application.

326 **4.2 Evolution of particle deposition at different coverage of defects**

327 To resolve the fine details for the role of membrane defects on fouling formantion and
328 development, Figure 4 displays the lateral particle deposition over the membrane
329 surface as a function of filtration time at different combined Φ_{md} & J_0, with the color
330 scale standing for the number of particles (#) attached in each simulation grid. For
331 perfect membranes (Φ_{md} = 0/50), particle deposition is very slow at a low J_0 of 10 μm/s
332 (Figure 4a$_1$). Only a dozen of particles per grid surfacing up on membrane are observed
333 after experiencing a long-term of 1000-min filtraion, thanks to the dominated role of
334 high F-M repulsion (see the curve of Φ_{md} = 0/50 in Figure 4a$_6$). Increasing J_0 to 20 and
335 30 μm/s while keeping Φ_{md} = 0/50 result in speeding up of foulants deposition (Figure
336 4b$_1$, c$_1$), accompanied by the transitional fouling behavior from high F-M to low F-F
337 (see the curves of Φ_{md} = 0/50 in Figure 4b$_6$, c$_6$). It is worthwhile to note that the

accelerated particles deposition starts at around 220 min and 20 min for J_0 of 20 and 30 μm/s, respectively, which agree well with their period of stable flux (Figure 3b, c). In the set of high E_m and low E_f, the initial deposited foulant patches reduce the local ΔE_b and serve as seeds for further foulant attachment. Owing to the stochastic nature of colloidal movement, the positions for intial foulant attachment are greatly random. Nevertheless, the foulant patches grow laterally over time, and a few new patches also surface up. Eventually, the entire membrane surface is completely covered by foulants, resulting in a F-F dominant interaction. Indeed, the initial foulant depositon curves for J_0 of 20 and 30 μm/s are nearly identical to that for ΔE_b fixed at 12 k_BT (implying a F-M control), while their fouling features at later stage are similar to that for ΔE_b fixed at 3 k_BT (meaning a F-F control) (see the curve of Φ_{md} = 0/50 in Figure 4b$_6$, c$_6$).

Unlike the defect-free membrane, a notable scenario of "taper-like" evolution of particle deposition is present for defective membranes (Figure 4 a$_2$-a$_4$, b$_2$-b$_4$, and c$_2$-c$_4$). Although the entire membrane with E_m = 12 k_BT exhibits worthy antifouling feature, the intrinsic defective spots with lowered energy barrier (E_{md} =6 k_BT) can serve as "nucleus" to promote deposition of particles in their vicinity owing to the weak F-F interaction. Consequently, the locations for initial particle deposition are highly selective, and hence a subulate-like "colonization" behavior is expected. Increasing Φ_{md} (*i.e.*, from 1/50 to 10/50) leads to the increased preferential spots for particle attachment, accompanied by the foulants deposition behavior tending to the low F-F interaction

(Figure 4 a6, b6, and c6). Our simulation echoes the existing literatures that the valleys of the rough membrane surface were favored to particles accumulation as a result of their low colloid-membrane repulsion [28-30].

A further close examination of particle deposition patterns indicates that the period of the selectivity for particle deposition is shortened with the increased initial flux. For instance, the hotspots for particle deposition exist the whole simulation time of 1000 min at J_0 = 10μm/s (Figure 4 a2–a4), while it is only about 100 min for the case of J_0 = 30μm/s (Figure 4 c2–c4). This is ascribed to the accelerated fouling shifting from F-M to F-F at greater J_0 (Figure 4 a6, b6 and c6). After membrane surface completely masked by foulants, fouling is controlled by low E_f, leading to the disappearance of selectivity in subsequent fouling stage.

As expected, fast particle deposition and much severe fouling occur for the case of Φ_{md} = 50/50 (Figure 4a5, b5, and c5), with more rapid fouling transition from F-D to F-F interaction at increased initial flux (Figure 4a6, b6, and c6). The accumulation of particle deposition for each segment reaches approximately 100 particles per grid (#/grid) in the initial 20 min, 3 min, and 2 min for J_0 of 10, 20 and 30 μm/s, respectively. Since the membrane surface is entirely covered by defects with low energy barreir (E_{md} = 6 k_BT), a relatively uniform foulant distribution patterns with nearly no selectivity are present.

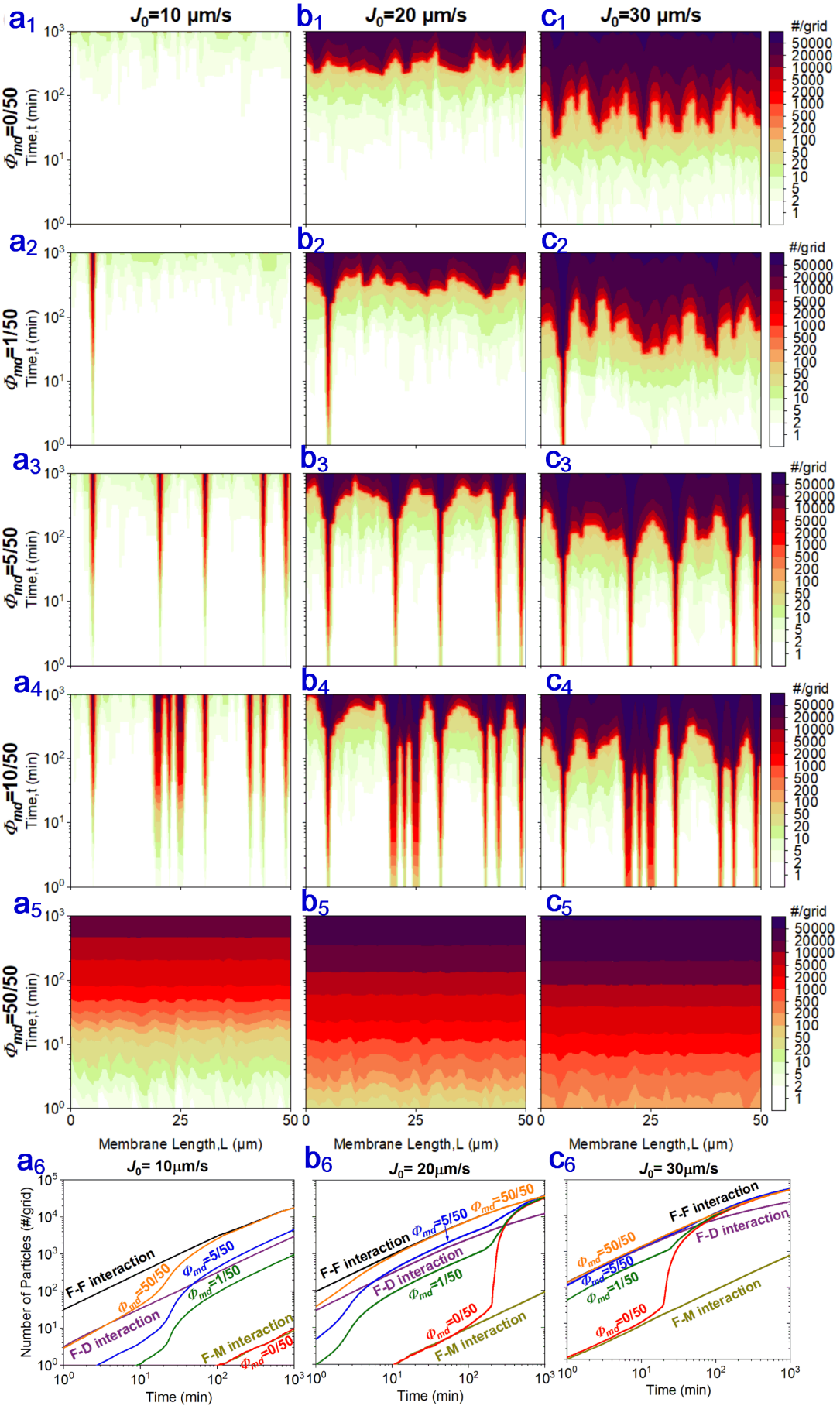
a1
J0=10 μm/s
b1
J0=20 μm/s
c1
J0=30 μm/s
#/grid
50000
20000
10000
5000
2000
1000
500
200
100
50
20
10
5
2
1
Φmd=0/50
Φmd=1/50
Φmd=5/50
Φmd=10/50
Φmd=50/50
Time,t (min)
Membrane Length,L (μm)
a6
J0= 10μm/s
b6
J0= 20μm/s
c6
J0= 30μm/s
Number of Particles (#/grid)
Time (min)
F-F interaction
F-D interaction
F-M interaction
Φmd=50/50
Φmd=5/50
Φmd=1/50
Φmd=0/50

379

Figure 4. Effect of coverage of membrane defects on the evolution of foulant deposition. Parts a_1-a_5, b_1-b_5, c_1-c_5 presents the particle deposition pattern over time at different combined E_{md} & J_0 values. The color scale stands for the number of particles (#) attachment in each simulation grid of 0.1 μm^2. Parts a_6, b_6 and c_6 shows the average particles accumulation of entire membrane surface over time. The solid lines are the mean values, in which the curves of F-M, F-D and F-F interaction represent the evolution of particle deposition at energy barrier fixed at E_m, E_{md}, and E_f, respectively. Simulation conditions: E_m = 12k_BT, E_{md} =6 k_BT, E_f = 3 k_BT, and the other modelling conditions listed in Table 1.

4.3 Water flux at different energy barrier of defects

To obtain a comprehensive understanding of the influences of defects, we further investigate the role of energy barrier of defects E_{md} on flux declines. With a J_0 of 20 μm/s, a negligible flux loss (<0.5%) occurs during the whole 1000-min duration at both high E_m (12 k_BT) and E_f (12 k_BT) regardless of E_{md} (Figure 5a). Even for the condition of E_{md} = 0 k_BT (*i.e.*, the locations of defects present no barrier in resiting particle depostion), the defect spots will be covered by the foulants to obtain a strong F-F repulsion that effectively retards further particle depositon. Such "self-terminated" fouling behavior also happens at lower E_m (9 k_BT or 3 k_BT) while keeping high E_f of 12 k_BT (Figure S3a, b of Supporting Information S4), and at reducing E_f to 9 k_BT while keeping E_m of 12 k_BT (insignificant flux loss < 4%, Figure 5b). Our simulation agrees well with the typical scenario reported by Wang et al. [45]. For example, the negatively charged NF membrane maintained a long-term stable flux after a sight drop in the initial stage during filtration of positively charged foulants, thanks to the strong F-F repulsion. Considering the fundamental importance of E_f, adjustments of feed pretreatment and

water chemistry are essential to gain strongly F-F repulsion for coping with defective membranes.

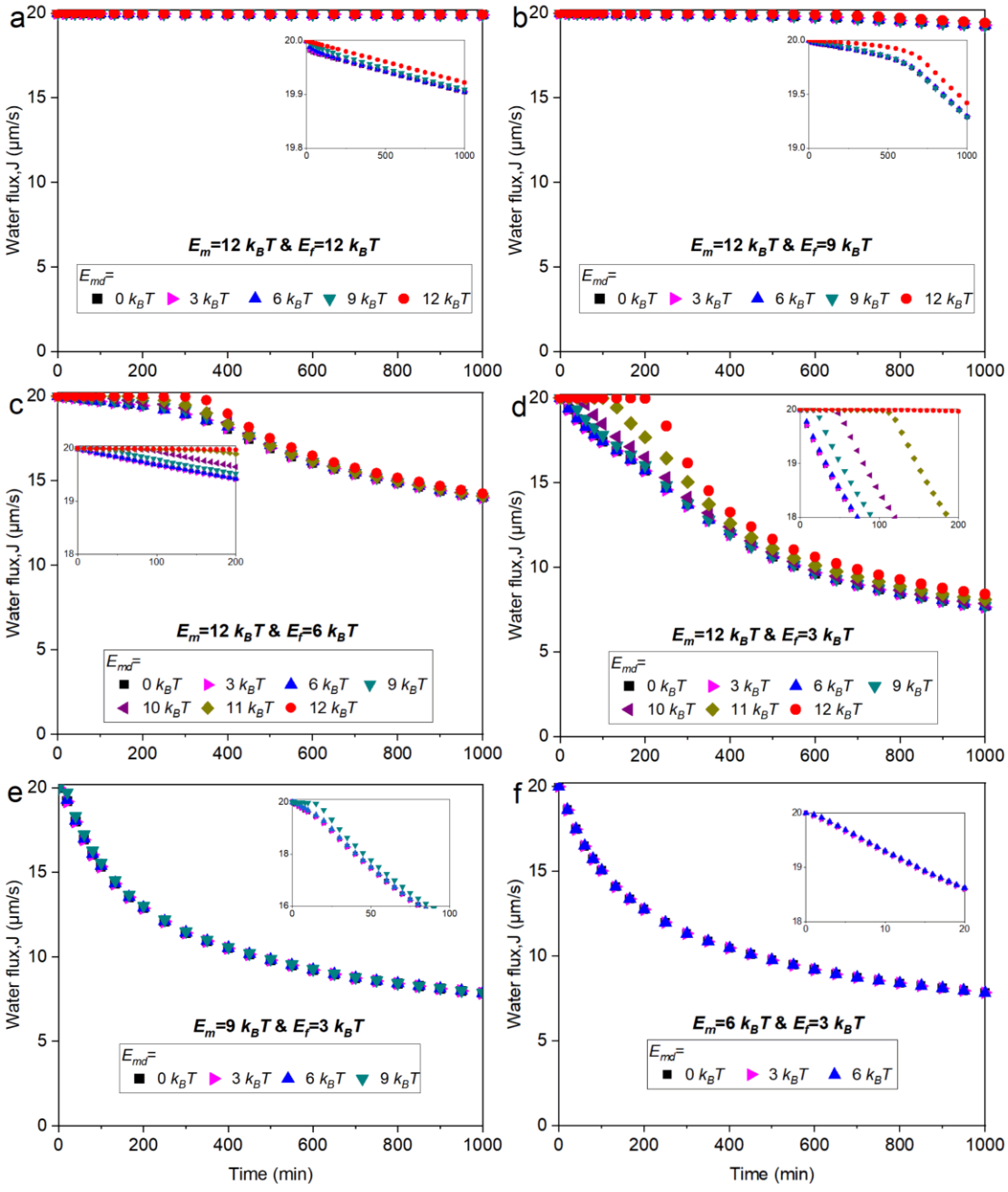

Figure 5. Effect of energy barrier of defects E_{md} on flux decline at different E_m & E_f combinations. Simulation conditions: J_0= 20 μm/s, E_{md} =0-12 k_BT, Φ_{md}=5/50, and other simulation conditions listed in Table 1.

Lowering E_f to 6 k_BT (Figure 5c) and 3 k_BT (Figure 5d) while keeping high E_m of 12 k_BT lead to more serious flux loss at the later fouling stage, which is attibuted to the

414 weak F-F repulsion. Nevertheless, due to the high F-M interaction, an initial stable flux
415 behavior is observed for $E_{md} > 6k_BT$, with reduced E_{md} leading to the shortened stable
416 duration (see the Insets of Figure 5c, d). Taking $E_f = 3\ k_BT$ (Figure 5d) as an example,
417 the duration of stable flux is about 220 min for membrane with defect-free ($E_{md} = E_m$
418 $=12\ k_BT$), while it reduces to half at $E_{md}=11\ k_BT$ and becomes almostly invisible for E_{md}
419 $\leq 6\ k_BT$. This simulation is supported by the experimental observations that metasble
420 flux is more salient for smooth membrane compared to other rough membrane [12].
421
422 Keeping $E_f = 3\ k_BT$ while lowering E_m to $9\ k_BT$ leads to much more severe fouling even
423 at the initial stage (Figure 5e), in which the role of defects on fouling is observed only
424 at the initial 20min. It is also interesting to find that further decresing E_m to $6\ k_BT$ while
425 maintaining the value of E_f leads to the identical and rapid flux declines at the begining
426 with/without defects (Figure 5f), which is attributed to the lack of robust repulsion of
427 both F-M and F-F in retarding foulant depositon. The simulations of Figure 5 d-f
428 underpin the fundenmental essentials to design a membrane with highly F-M repulsion
429 to obtain extended period of matestable flux.
430

431 **4.4 Evolution of particle deposition at different energy barrier of defects**

432 To deeply dissect the effect of E_m on fouling, we further plot the evolution of particle
433 deposition patterns at different combination of E_m & E_f(Figure 6). As expected, particle

accumulation on the membrane is much slow at both high E_m (12 k_BT) and E_f (12 k_BT) for defect-free membrane (Figure 6a$_1$). The average value is approx. 100 #/grid during the whole 1000-min duration (Figure 6a$_3$), thanks to the strongly repulsion of both F-M and F-F. While for defective membrane (Figure 6a$_2$), a rapid initial particle deposition on the local positions is observed, reaching more than 100 #/grid in the first 2 min due to the weak F-D intereaction. However, the subsequent accumulation of foulants at the local defects is extremely slow (slightly over 300 #/grid at the end of the 1000-min duration), thank to the rapid conditioning of the local defects by the attached particles, resulting in a more repulsive F-F interaction (Figure 6a$_3$). In this condition, the deposited foulants can act as a patching to timely repair the defects, avoiding the occurrence of substantial flux decline (Figure 5a). Indeed, the fouling behavior of defective membrane is progressively far away from that of F-D interaction but increasingly approaches to that of defect-free membrane (*i.e.*, F-M and F-F interaction) as the filtration time going on (Figure 6a$_3$). Our simulation suggests that a strong F-F repulsion can ensure long-term stable water flux regardless of the existence of membrane defects, consolidating the vital importance of modifying the water characteristics (*e.g.*, via pretreating feed and adjusting solution chemistry [14, 45, 46]) to enhance F-F interaction in real application.

Lowering E_f from 12 to 6, 3 k_BT while maintaining E_m at 12 k_BT weakens “repairing” effect but gradually strengthens “seeding” effect, which is reflected by the increasingly

intensitied selectivity of foulant accumulation on the local defects (Figure 6 b_1-b_2, c_1-c_2). For example, the number of particles attached on the defective grids in inital 100 min is about 210-220 #/grid at E_f = 12 k_BT, while it increases by an order of magnitude at decreased E_f and reaches around 3620, 35500 #/grid for E_f of 6, 3 k_BT, respectively. Furthermore, the accelarated foulant accumulation on defective spots at lowered E_f results in premature shifting of particle depostion behavior towards F-F interaction (Figure 6 b_3, c_3), accompanied by the substianal flux drops compared to that of defect-free membrane (Figure 5c, d).

When E_f fixed at 3 k_BT, it is interesting to observe that decreased E_m from 12 to 9 and 6 k_BT leads to the shortened period of hotspot selectivity (Figure 6 c_1-c_2, d_1-d_2, e_1-e_2). Specifically, the influence of defect on particle deposition evolution can maintain several hundred minutes at E_m of 12 k_BT, while it only works a few dozen min for E_m =9 k_BT, and a couple min for E_m =6 k_BT. This can be explained by the accelerated starting time of fouling transiton from F-M to F-F at decreased E_m, thereby shrinking the influence of the local defects on particle deposition (Figure 6 c_3, d_3, e_3).

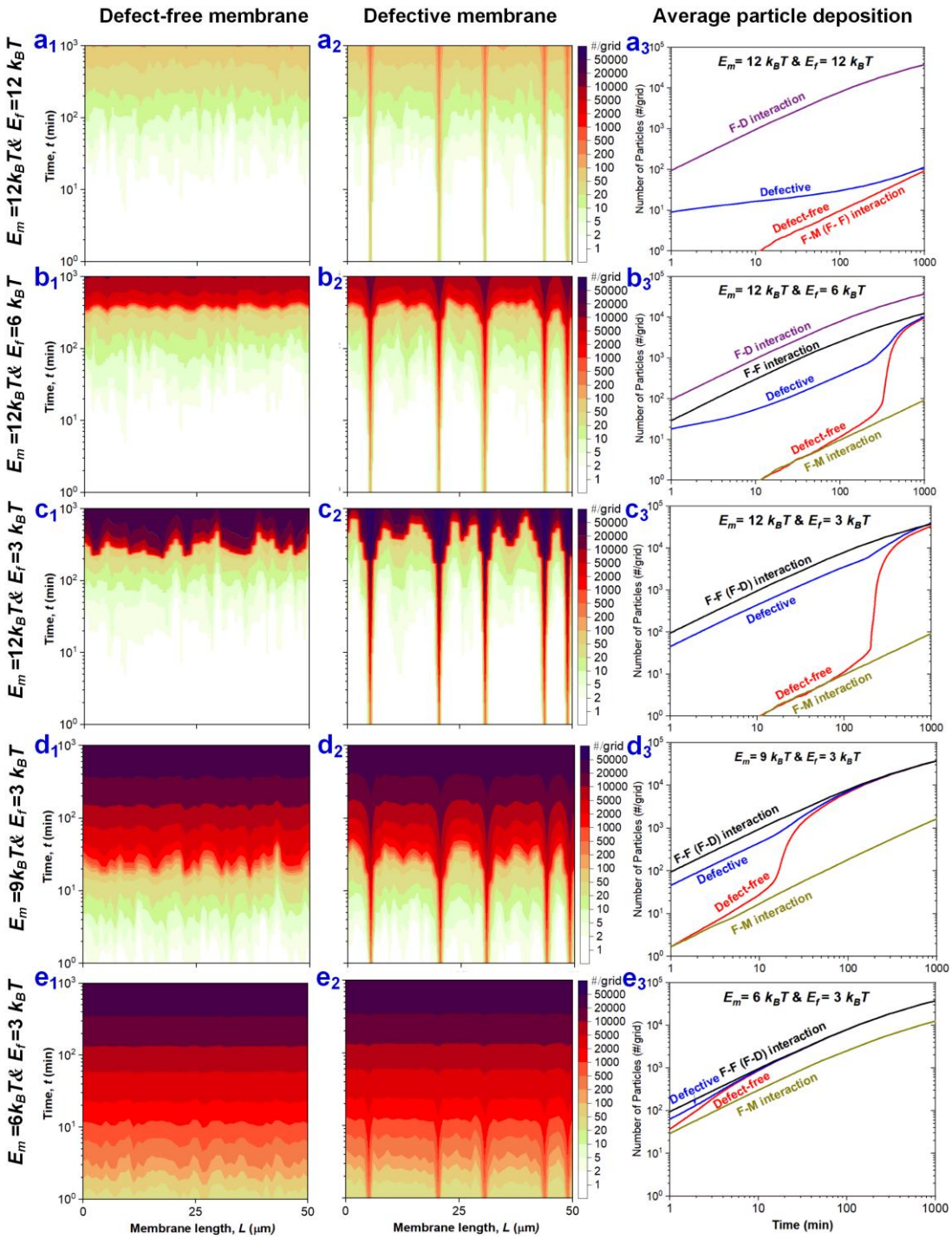

Figure 6. Effect of energy barrier of defects on the evolution of particle deposition. The left and middle parts (a_1-a_2, b_1-b_2, c_1-c_2, d_1-d_2, and e_1-e_2) present the particle deposition patterns over time at different E_m & E_f combinations. The color scale represents the number of particles (#) attachment in each grid of 0.1 μm^2. The right parts (a_3, b_3, c_3, d_3, and e_3) present the average particles accumulation of the entire membrane as a function of time. The solid lines are the mean values, in which the curves of F-M, F-D and F-F interaction represent the evolution of particle deposition at energy barrier fixed at E_m, E_{md}, and E_f, respectively. Simulation conditions: Φ_{md} =5/50, E_{md} =3 k_BT, J_0= 20 μm/s, and the other modelling conditions listed in Table 1.

4.5 Role of membrane defects on initial fouling rate

According to above simulations, membrane defects have significant influences on initial fouling process. To achieve a better understanding of the role of defects, we plot the initial fouling rate dm_f/dt (*i.e.*, rate of particle deposition, in μg/m^{2}s) as a function coverage of defects Φ_{md} at different initial flux and colloid-membrane interaction. Under low and medium initial flux (J_0<30μm/s), Figure 7a clearly shows that increasing Φ_{md} (from 50/50 to 0/50) leads to the progressively increased dm_f/dt by orders of magnitudes (*i.e.*, ranging from ~10 to < 0.01 μg/m^{2}s), which is attributed to the elevated probability of successful particle attachment α as a result of the decreased colloid-surface repulsion (Eq. 3). While for relatively higher J_0 (>30μm/s), the influence of Φ_{md} on dm_f/dt is less discernible, which can be explained that greater J_0 can give rise to larger transport velocity (Eq. 2), more collision frequency (Eq. S1) as well as higher attachment coefficient (Eq. 3). As a result, each collision event can lead to successful attachment regardless of the variation of colloid-surface interaction induced by local defects. The simulation results are in consistent with the less distinct effect of Φ_{md} on fouling at higher initial flux (Figure 3a-c). The role of Φ_{md} on initial dm_f/dt is also highly affected by F-M (Figure 7b) and F-D interaction (Figure 7c). At high E_m(>12 k_BT) or low E_{md} (< 6 k_BT), the effect of Φ_{md} is salient that fouling rate increases by one order of magnitude for every increase of defective segments by < 20 grids. However, it is less obvious at low E_m (≤ 8 k_BT) or high E_{md} (≥ 10 k_BT), with dm_f/dt increasing by less than one order of magnitude over the whole range of Φ_{md} (from 0/50 to 50/50). Indeed,

lowered E_m or increased E_{md} reduces the difference between F-M and F-D interactions, further leading to the diminished influences of Φ_{md}.

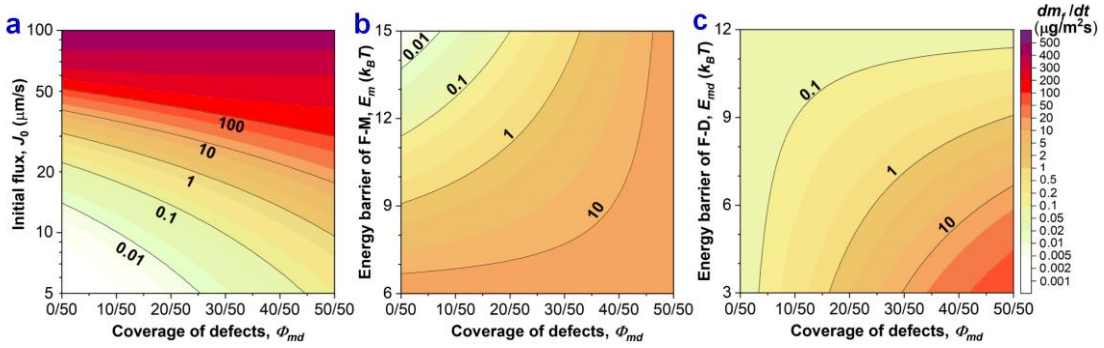

Figure 7. Effect of Φ_{md} on initial fouling rate at variation of (a) J_0, (b) E_m, and (c) E_{md}. Simulation parameters: J_0 = 20 μm/s, E_m = 12 k_BT, and E_{md} = 6 k_BT. The color scale represents the initial rate of foulant deposition (dm_f/dt, in μg/m^{2}s) calculated based on the CA theory equations (Supporting Information S5).

4.6 Critical energy barrier

Figure 5a-c reveal that there seems to be a critical energy barrier (E_c) for F-F interaction, above which little or minimal fouling occurs during the long-term filtration and the presence of defects has negligible influence on fouling. Meanwhile, the flux behaviors of Figure 5d-f disclose that there is likely to be a threshold of E_c for F-M interaction, above which an initial extended metastable flux appears for defect-free membrane, with the existence of defects leading to shortened metastable period and thus accelerating fouling. Essentially, the critical energy barrier is related to the well-known concept of critical flux (or limiting flux), which states that little/no fouling happens when membrane flux below a threshold value [18, 41, 47]. According to CA theory, the E_c can be operationally defined as the water flux corresponding to a much small rate of fouling dm_f/dt. By using a threshold dm_f/dt of 1 μg/m^{2}s [16, 44], Figure 8a plots the E_c

as a function of J_0. As expected, a small E_c is observed at low flux (≤ 5 μm/s). Increased J_0 leads to a nearly linear dependence of E_c on flux for J_0 > 5 μm/s. For instance, the value of E_c is about 6.1, 9.0, and 11.7 k_BT for J_0 of 10, 20, and 30 μm/s, respectively. Indeed, a larger J_0 exerts greater hydrodynamic drag on particle, which requires a higher E_c to decrease α and thus to meet the anticipated fouling rate. In practical implication, the critical energy barrier is fundamentally important. For a given operation flux (or a demand water production), the value of E_c can be viewed as an anticipated criterion for membrane design and feedwater pretreatment to obtain an extended metastable flux or even a long-term stable flux.

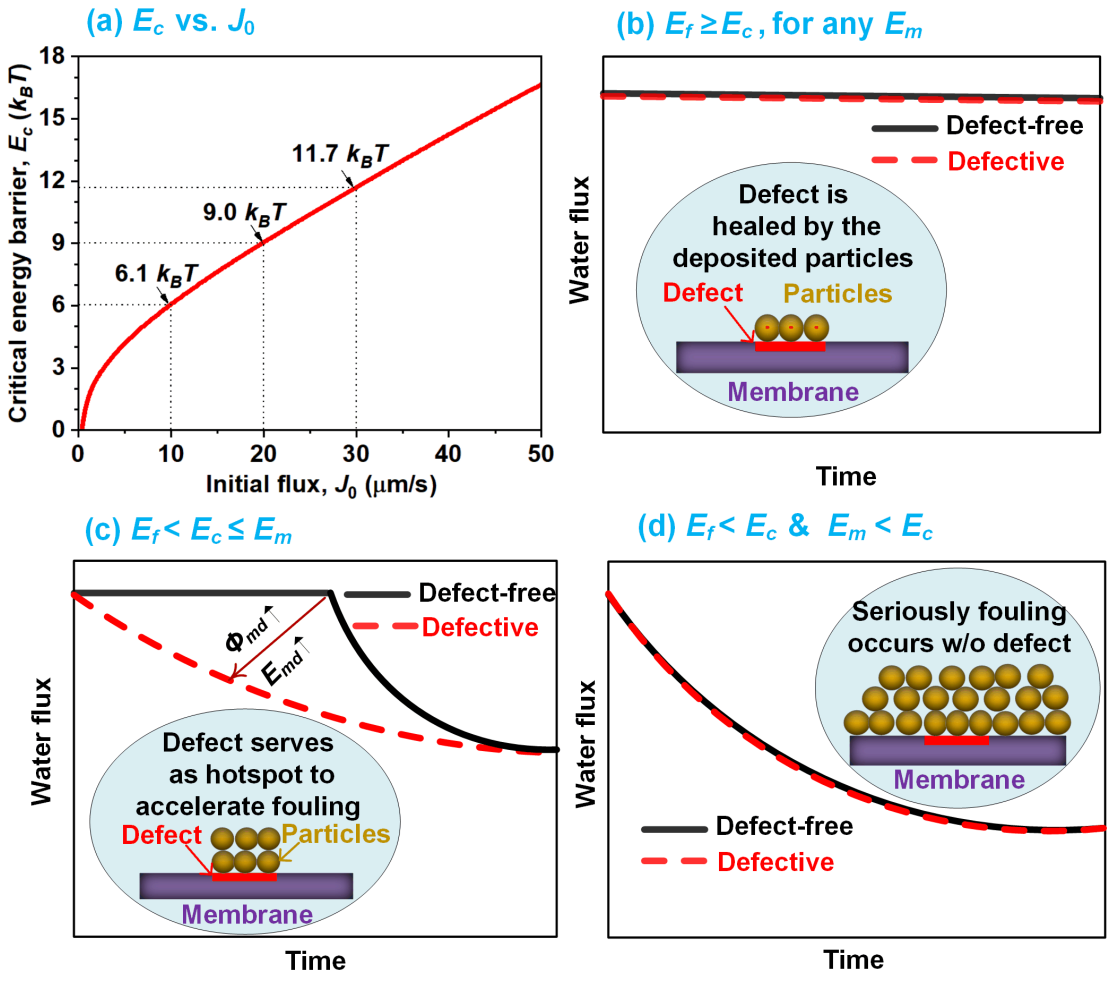

Figure 8. Critical energy barrier and its importance on fouling. Part (a) presents the

532 critical energy barrier E_c as a function of water flux J_0. The value of E_c is calculated
533 according the CA theory equations by using 1 μg/m^{2}s as a threshold dm_f/dt [16, 44].
534 Parts (b-d) present conceptual influence of membrane defect on fouling at (b) $E_f \geq E_c$,
535 for any E_m; (c) $E_f < E_c \leq E_m$; and (d) $E_f < E_c$ & $E_m < E_c$.
536
537 More importantly, the introduction of the concept of critical energy barrier in this work
538 allows us to dissect the critical role of membrane defects based on the relative
539 magnitudes of E_f, E_m and E_c. For any given J_0, membrane defects influencing on fouling
540 can be divided into the following three cases:

541 ● $E_f \geq E_c$ (see Figure 8b). As a result of strong F-F repulsion, the initial attached
542 foulants on the defective spots can be viewed as "patches" to timely repair the
543 defects, effectively preventing further particles deposition. In this case, membrane
544 flux remains stable at a relatively long-term duration and negligible fouling
545 happens, regardless of the presence of defects (Figure 5a, b and Figure S3a, b).

546 ● $E_f < E_c \leq E_m$ (see Figure 8c). Owing to the high F-M interaction, there appears to
547 be a metastable flux in the initial stage for defect-free membrane. Its stable period
548 is highly dependent on the surplus of E_m over E_c. For example, the initial stable
549 flux can merely maintain about 20 min at $E_m \approx E_c$ (*i.e.*, Figure 3c and Figure 5e).
550 Whereas, more extended periods (several hundred min) are observed at enlarged
551 difference between E_m and E_c (*i.e.*, $E_m - E_c = 5.9\ k_BT$ in Figure 3a; and $E_m - E_c = 3.0$
552 k_BT in Figure 3b, & Figure 5c, 5d). For defective membrane, the initial foulants
553 preferential deposition on the defective spots serve as "nucleus", greatly favoring
554 further particles attachment in their vicinity owing to the low F-F interaction.
555 Consequently, the existence of local defects can accelerate fouling, with increased

Φ_{md} or decreased E_{md} leading to decrease or even disappearance of metastable period (Figure 3a-3c and Figure 5c-d).

- $E_m < E_c$ & $E_f < E_c$ (see Figure 8d). Since both F-M and F-F are lack of robust resistance against particle deposition, rapid transition (*i.e.*, from F-M to F-F) occurs even at the first couple of minutes (Figure 6e$_1$, e$_2$), accompanied by the rapid flux decline (Figure 5f). In this condition, serious fouling occurs with/without defects.

5 Conclusion and implications

For the first time, this work comprehensively investigates the critical role of membrane defects with spatial variability of foulant-membrane interaction on fouling by adopting a CA-MC model that captures the fine details of particle transport, collision and attachment. Simulation results show that effect of membrane defects on fouling is highly governed by energy barreirs of both F-M and F-F. When the value of E_f exceeds a threshold value, *i.e.*, E_c, the long-term water flux remains stable regardless of the existence of local defects. At the condition of high E_m ($\geq E_c$) and low E_f ($<E_c$), there appears to be an extended metastable flux for defect-free membrane, with increased Φ_{md} and lowered E_{md} leading to decrease or even disappearance of metastable flux period. For both low E_f ($<E_c$) and E_m ($<E_c$), severe fouling occurs at the beginning of filtration with/without defects. Furthermore, effect of membrane defects become less discernible at higher initial flux where hydrodynamic drag prevails. Our simulations can reconcile the existing contradictory experimental phenomena in literatures

577 regarding the defects influencing on fouling.

578

579 Traditionally, Navier-Stokes (NS) -based fouling models were widely adopted to
580 simulate the colloidal transport in the hydrodynamic boundary layer [48, 49]. But a key
581 challenge for application of NS equation is that the colloid- surface interaction force as
582 well as pressure force and viscous force exert at different magnitude scales [14, 50, 51].
583 Although some simpler models, e.g., concentration polarization [52-54] and mass
584 transfer [55-57] have been put forward in the past few decades, these models often
585 neglect the role of colloid - membrane interaction on fouling. With the ongoing
586 advancement in computational program and artificial intelligence, the application of
587 artificial neural networks (ANN) for prediction of fouling has attracted much attention
588 in membrane field over the recent years [58]. Due to the powerful capability to
589 autonomously learn and recognize trends within a series of input and output data, ANN
590 can forecast the complex non-linear relationships among variables and their influences
591 on fouling during membrane filtration processes [59, 60]**.** Despite significant advances
592 achieved, there are still some serious concerns in implementing ANN for predicting
593 membrane fouling, including (1) poor reproducibility owing to the random weight and
594 bias between neurons [61], (2) time-consuming process as a result of training and
595 testing large amounts of data [62], and (3) lack of mechanistic insights due to the
596 "black-box" nature of ANN models [58]. Compared to the above NS models and ANN
597 simulations, the CA-MC approach adopted herein not only presents a strong physical

598 basis for the understanding of the role of colloid-membrane interaction and
599 hydrodynamics interaction on membrane fouling, but also provides a facile algorithm
600 procedure for simulation.
601
602 Our simulations have important implications for membrane design and feed
603 pretreatment. The development of smooth membranes with minimal defects is essential
604 to achieve a better antifouling ability with extended metastable flux period. However,
605 it should be noticed that membrane defects are often unavoidable in membrane
606 preparation [1, 22]. For applications with defective membranes, it is a useful strategy to
607 pretreat problematic feed to enhance F-F repulsion and thus to effectively resist paticles
608 deposition as a result of the "self-healing" behavior for the defect spots. Furthermore,
609 excessively high operating flux should be seriously prohibited as it can accelerate
610 foulants accumulation on the defect spots and thereby promoting transition from high
611 F-M to low F-F owing to the higher permeate drag, which also requires a higher
612 threshold energy barrier E_c in resisting fouling (Figure 8a). In practice, application of
613 low to moderate flux is often recommended in seawater desalination (12-17 L m^{-2} h^{-1})
614 and brackish water treatment (12-45 L m^{-2} h^{-1}) [63].
615
616 Our results also reveal the crucial influence of the foulant propagation at the defect
617 regions in worsening the membrane performace. For example, despite that most of the
618 memrbane surface is still clean in the initial 200-min period for Φ_{md} in the range of 1/50

to 5/50 at J_0=10 μm/s (Figure 4a$_2$,a$_3$) and J_0=20 μm/s (Figure 4b$_2$,b$_3$), substantial flux declines are obseved (Figure 3a, b). Therefore, once the foulant patches initially appear, timely cleaning on the defective positions is of great importance to avoid excessive "colonization" of deposited foulants and to recover the water flux. While the extensive literature focused on cleaning methods and chemical agents, future work should emphasize on the timing and the locations of cleaning.

Acknowledgements

This study was financially supported by the National Key Research and Development Program of China (2021YFC3201401), Science and Technology Planning Project of Guangdong Province (2021A0505110013), National Natural Science Foundation of China (42107431 and 51708130), and Seed Fund for Basic Research by the University of Hong Kong (104005856).

References

[1] Z. Yang, P.F. Sun, X. Li, B. Gan, L. Wang, X. Song, H.D. Park, C.Y. Tang, A critical review on thin-film nanocomposite membranes with interlayered structure: Mechanisms, recent developments, and environmental applications, Environ. Sci. Technol. 54(24) (2020) 15563-15583. https://doi.org/10.1021/acs.est.0c05377.

[2] M. Qasim, M. Badrelzaman, N.N. Darwish, N.A. Darwish, N. Hilal, Reverse osmosis desalination: A state-of-the-art review, Desalination 459 (2019) 59-104. https://doi.org/10.1016/j.desal.2019.02.008.

[3] W. Yin, X. Li, S.R. Suwarno, E.R. Cornelissen, T.H. Chong, Fouling behavior of isolated dissolved organic fractions from seawater in reverse osmosis (RO) desalination process, Water Res. 159 (2019) 385-396. https://doi.org/10.1016/j.watres.2019.05.038.

[4] C.Y. Tang, Z. Yang, H. Guo, J.J. Wen, L.D. Nghiem, E. Cornelissen, Potable water reuse through advanced membrane technology, Environ. Sci. Technol. 52(18) (2018) 10215-10223. https://doi.org/10.1021/acs.est.8b00562.

[5] M.F. Tay, S. Lee, H. Xu, K. Jeong, C. Liu, E.R. Cornelissen, B. Wu, T.H. Chong, Impact of salt accumulation in the bioreactor on the performance of nanofiltration membrane bioreactor (NF-MBR) plus Reverse osmosis (RO) process for water reclamation, Water Res. 170 (2020) 115352. https://doi.org/10.1016/j.watres.2019.115352.
[6] H. Guo, X. Li, W. Yang, Z. Yao, Y. Mei, L.E. Peng, Z. Yang, S. Shao, C.Y. Tang, Nanofiltration for drinking water treatment: a review, Front. Chem. Sci. Eng. 16(5) (2022) 681-698. https://doi.org/10.1007/s11705-021-2103-5.
[7] Z.Y. Su, T. Liu, X. Li, N. Graham, W.Z. Yu, Beneficial impacts of natural biopolymers during surface water purification by membrane nanofiltration, Water Res. 201 (2021) 117330. https://doi.org/10.1016/j.watres.2021.117330.
[8] Y. Xiao, D. Guo, T. Li, Q. Zhou, L. Shen, R. Li, Y. Xu, H. Lin, Facile fabrication of superhydrophilic nanofiltration membranes via tannic acid and irons layer-by-layer self-assembly for dye separation, Appl. Surf. Sci. 515 (2020) 146063. https://doi.org/10.1016/j.apsusc.2020.146063.
[9] N.K. Khanzada, M.U. Farid, J.A. Kharraz, J. Choi, C.Y. Tang, L.D. Nghiem, A. Jang, A.K. An, Removal of organic micropollutants using advanced membrane-based water and wastewater treatment: A review, J. Membr. Sci. 598 (2020) 117672. https://doi.org/10.1016/j.memsci.2019.117672.
[10] C.Y. Tang, T.H. Chong, A.G. Fane, Colloidal interactions and fouling of NF and RO membranes: A review, Adv. Colloid Interface Sci. 164(1-2) (2011) 126-143. https://doi.org/10.1016/j.cis.2010.10.007.
[11] C.Y. Tang, Y.-N. Kwon, J.O. Leckie, Fouling of reverse osmosis and nanofiltration membranes by humic acid—Effects of solution composition and hydrodynamic conditions, J. Membr. Sci. 290(1) (2007) 86-94. https://doi.org/10.1016/j.memsci.2006.12.017.
[12] Y.N. Wang, C.Y. Tang, Protein fouling of nanofiltration, reverse osmosis, and ultrafiltration membranes-The role of hydrodynamic conditions, solution chemistry, and membrane properties, J. Membr. Sci. 376(1-2) (2011) 275-282. https://doi.org/10.1016/j.memsci.2011.04.036.
[13] Z. Jiang, S. Karan, A.G. Livingston, Membrane Fouling: Does Microscale Roughness Matter?, Ind. Eng. Chem. Res. 59(12) (2020) 5424-5431. https://doi.org/10.1021/acs.iecr.9b04798.
[14] C.Y. Tang, Y.N. Kwon, J.O. Leckie, The role of foulant–foulant electrostatic interaction on limiting flux for RO and NF membranes during humic acid fouling—Theoretical basis, experimental evidence, and AFM interaction force measurement, J. Membr. Sci. 326(2) (2009) 526-532. https://doi.org/10.1016/j.memsci.2008.10.043.
[15] J. Liu, T. Huang, R. Ji, Z. Wang, C.Y. Tang, J.O. Leckie, Stochastic collision–attachment-based monte carlo simulation of colloidal fouling: Transition from foulant–clean-membrane interaction to foulant–fouled-membrane interaction, Environ. Sci. Technol. 54(19) (2020) 12703-12712.

https://doi.org/10.1021/acs.est.0c04165.
[16] J. Liu, Y. Fan, Y. Sun, Z. Wang, D. Zhao, T. Li, B. Dong, C.Y. Tang, Modelling the critical roles of zeta potential and contact angle on colloidal fouling with a coupled XDLVO - collision attachment approach, J. Membr. Sci. 623 (2021) 119048. https://doi.org/10.1016/j.memsci.2021.119048.
[17] D.Y. Li, W.C. Lin, R.P. Shao, Y.X. Shen, X.Z. Zhu, X. Huang, Interaction between humic acid and silica in reverse osmosis membrane fouling process: A spectroscopic and molecular dynamics insight, Water Res. 206 (2021) 117773. https://doi.org/10.1016/j.watres.2021.117773.
[18] C.Y. Tang, J.O. Leckie, Membrane independent limiting flux for RO and NF membranes fouled by humic acid, Environ. Sci. Technol. 41(13) (2007) 4767-4773. https://doi.org/10.1021/es063105w.
[19] J. Liu, Z. Wang, C.Y. Tang, J.O. Leckie, Modeling dynamics of colloidal fouling of RO/NF membranes with a novel collision-attachment approach, Environ. Sci. Technol. 52(3) (2018) 1471-1478. https://doi.org/10.1021/acs.est.7b05598.
[20] L. Shan, H. Fan, H. Guo, S. Ji, G. Zhang, Natural organic matter fouling behaviors on superwetting nanofiltration membranes, Water Res. 93 (2016) 121-132. https://doi.org/10.1016/j.watres.2016.01.054.
[21] D. Ankoliya, B. Mehta, H. Raval, Advances in surface modification techniques of reverse osmosis membrane over the years, Sep. Sci. Technol. 54(3) (2019) 293-310. https://doi.org/10.1080/01496395.2018.1483404.
[22] M. Ulbricht, Advanced functional polymer membranes, Polymer 47(7) (2006) 2217-2262. https://doi.org/10.1016/j.polymer.2006.01.084.
[23] J.M. Ochando-Pulido, A. Martínez-Ferez, Fouling modelling on a reverse osmosis membrane in the purification of pretreated olive mill wastewater by adapted crossflow blocking mechanisms, J. Membr. Sci. 544 (2017) 108-118. https://doi.org/10.1016/j.memsci.2017.09.018.
[24] J.M. Ochando-Pulido, M.D. Víctor-Ortega, A. Martínez-Ferez, Membrane fouling insight during reverse osmosis purification of pretreated olive mill wastewater, Sep. Purif. Technol. 168 (2016) 177-187. https://doi.org/10.1016/j.seppur.2016.05.024.
[25] X. Song, B. Gan, S. Qi, H. Guo, C.Y. Tang, Y. Zhou, C. Gao, Intrinsic nanoscale structure of thin film composite polyamide membranes: Connectivity, defects, and structure–property correlation, Environ. Sci. Technol. 54(6) (2020) 3559-3569. https://doi.org/10.1021/acs.est.9b05892.
[26] C.Y. Tang, Y.-N. Kwon, J.O. Leckie, Characterization of humic acid fouled reverse osmosis and nanofiltration membranes by transmission electron microscopy and streaming potential measurements, Environ. Sci. Technol. 41(3) (2007) 942-949. https://doi.org/10.1021/es061322r.
[27] L.E. Peng, Z. Yao, Z. Yang, H. Guo, C.Y. Tang, Dissecting the role of substrate on the morphology and separation properties of thin film composite polyamide membranes: Seeing is believing, Environ. Sci. Technol. 54(11) (2020) 6978-6986. https://doi.org/10.1021/acs.est.0c01427.

[28] M. Elimelech, Z. Xiaohua, A.E. Childress, H. Seungkwan, Role of membrane surface morphology in colloidal fouling of cellulose acetate and composite aromatic polyamide reverse osmosis membranes, J. Membr. Sci. 127(1) (1997) 101-109. https://doi.org/10.1016/S0376-7388(96)00351-1.
[29] E.M. Vrijenhoek, S. Hong, M. Elimelech, Influence of membrane surface properties on initial rate of colloidal fouling of reverse osmosis and nanofiltration membranes, J. Membr. Sci. 188(1) (2001) 115-128. https://doi.org/10.1016/s0376-7388(01)00376-3.
[30] E.M.V. Hoek, S. Bhattacharjee, M. Elimelech, Effect of membrane surface roughness on colloid−membrane DLVO interactions, Langmuir 19(11) (2003) 4836-4847. https://doi.org/10.1021/la027083c.
[31] D. Thomas, S. Judd, N. Fawcett, Flocculation modelling: a review, Water Res. 33(7) (1999) 1579-1592. https://doi.org/10.1016/S0043-1354(98)00392-3.
[32] L.D. Landau, E.M. Lifshitz, CHAPTER IV - IDEAL GASES, in: L.D. Landau, E.M. Lifshitz (Eds.), Statistical Physics (Third Edition), Butterworth-Heinemann, Oxford, 1980, pp. 111-157. https://doi.org/10.1016/B978-0-08-057046-4.50011-7.
[33] M. Stoller, On the effect of flocculation as pretreatment process and particle size distribution for membrane fouling reduction, Desalination 240(1) (2009) 209-217. https://doi.org/ 10.1016/j.desal.2007.12.042.
[34] W.J. Lau, P.S. Goh, A.F. Ismail, S.O. Lai, Ultrafiltration as a pretreatment for seawater desalination: A review, Membr. Water Treat. 5(1) (2014) 15-29. https://doi.org/10.12989/mwt.2014.5.1.015.
[35] S.F. Anis, R. Hashaikeh, N. Hilal, Reverse osmosis pretreatment technologies and future trends: A comprehensive review, Desalination 452 (2019) 159-195. https://doi.org/10.1016/j.desal.2018.11.006.
[36] P. Bacchin, P. Aimar, R.W. Field, Critical and sustainable fluxes: Theory, experiments and applications, J. Membr. Sci. 281(1-2) (2006) 42-69. https://doi.org/10.1016/j.memsci.2006.04.014.
[37] G. Belfort, R.H. Davis, A.L. Zydney, The behavior of suspensions and macromolecular solutions in crossflow microfiltration, J. Membr. Sci. 96(1) (1994) 1-58. https://doi.org/10.1016/0376-7388(94)00119-7.
[38] P. Aimar, P. Bacchin, Slow colloidal aggregation and membrane fouling, J. Membr. Sci. 360(1-2) (2010) 70-76. https://doi.org/10.1016/j.memsci.2010.05.001.
[39] D. Krapf, Chapter Five - Mechanisms underlying anomalous diffusion in the plasma membrane, in: A.K. Kenworthy (Ed.), Curr. Top. Membr., Academic Press 2015, pp. 167-207. https://doi.org/10.1016/bs.ctm.2015.03.002.
[40] S. Hong, M. Elimelech, Chemical and physical aspects of natural organic matter (NOM) fouling of nanofiltration membranes, J. Membr. Sci. 132(2) (1997) 159-181. https://doi.org/10.1016/S0376-7388(97)00060-4.
[41] R. Field, D. Wu, J. Howell, B. Gupta, Critical flux concept for microfiltration fouling, J. Membr. Sci. 100(3) (1995) 259-272. https://doi.org/10.1016/0376-7388(94)00265-Z.

[42] M.C. Porter, Concentration polarization with membrane ultrafiltration, Ind Eng Chem. Prod. Res. Dev. 11(3) (1972) 234-248. https://doi.org/10.1021/i360043a002.
[43] J. Wang, L. Wang, R. Miao, Y. Lv, X. Wang, X. Meng, R. Yang, X. Zhang, Enhanced gypsum scaling by organic fouling layer on nanofiltration membrane: Characteristics and mechanisms, Water Res. 91 (2016) 203-213. https://doi.org/10.1016/j.watres.2016.01.019.
[44] J. Liu, Y. Zhao, Y. Fan, H. Yang, Z. Wang, Y. Chen, C.Y. Tang, Dissect the role of particle size through collision-attachment simulations for colloidal fouling of RO/NF membranes, J. Membr. Sci. 638 (2021) 119679. https://doi.org/10.1016/j.memsci.2021.119679.
[45] Y.N. Wang, C.Y. Tang, Fouling of nanofiltration, reverse osmosis, and ultrafiltration membranes by protein mixtures: the role of inter-foulant-species interaction, Environ. Sci. Technol. 45(15) (2011) 6373-6379. https://doi.org/10.1021/es2013177.
[46] W. Gao, H. Liang, J. Ma, M. Han, Z.l. Chen, Z.S. Han, G.B. Li, Membrane fouling control in ultrafiltration technology for drinking water production: A review, Desalination 272(1) (2011) 1-8. https://doi.org/10.1016/j.desal.2011.01.051.
[47] T. Nguyen, C. Lee, R. Field, I. Kim, Insight into organic fouling behavior in polyamide thin-film composite forward osmosis membrane: Critical flux and its impact on the economics of water reclamation, J. Membr. Sci. 606 (2020) 118118. https://doi.org/10.1016/j.memsci.2020.118118.
[48] R. Ghidossi, D. Veyret, P. Moulin, Computational fluid dynamics applied to membranes: State of the art and opportunities, Chem. Eng. Process. 45(6) (2006) 437-454. https://doi.org/10.1016/j.cep.2005.11.002.
[49] G. Belfort, Fluid mechanics in membrane filtration: recent developments, J. Membr. Sci. 40(2) (1989) 123-147. https://doi.org/10.1016/0376-7388(89)89001-5.
[50] J.A. Brant, A.E. Childress, Assessing short-range membrane–colloid interactions using surface energetics, J. Membr. Sci. 203(1) (2002) 257-273. https://doi.org/10.1016/S0376-7388(02)00014-5.
[51] E.M.V. Hoek, A.S. Kim, M. Elimelech, Influence of crossflow membrane filter geometry and shear rate on colloidal fouling in reverse osmosis and nanofiltration separations, Environ. Eng. Sci. 19(6) (2002) 357-372. https://doi.org/10.1089/109287502320963364.
[52] K. Madireddi, R. Babcock, B. Levine, J. Kim, M. Stenstrom, An unsteady-state model to predict concentration polarization in commercial spiral wound membranes, J. Membr. Sci. 157(1) (1999) 13-34. https://doi.org/10.1016/S0376-7388(98)00340-8.
[53] M. Amokrane, D. Sadaoui, C. Koutsou, A. Karabelas, M. Dudeck, A study of flow field and concentration polarization evolution in membrane channels with two-dimensional spacers during water desalination, J. Membr. Sci. 477 (2015) 139-150. https://doi.org/10.1016/j.memsci.2014.11.029.
[54] X. Li, M. Younas, M. Rezakazemi, Q.V. Ly, J. Li, A review on hollow fiber

membrane module towards high separation efficiency: Process modeling in fouling perspective, Chin. Chem. Lett. 33(8) (2022) 3594–3602. https://doi.org/10.1016/j.cclet.2021.10.044.
[55] J. Santos, V. Geraldes, S. Velizarov, J. Crespo, Investigation of flow patterns and mass transfer in membrane module channels filled with flow-aligned spacers using computational fluid dynamics (CFD), J. Membr. Sci. 305(1) (2007) 103-117. https://doi.org/10.1016/j.memsci.2007.07.036.
[56] C. Koutsou, S. Yiantsios, A. Karabelas, A numerical and experimental study of mass transfer in spacer-filled channels: effects of spacer geometrical characteristics and Schmidt number, J. Membr. Sci. 326(1) (2009) 234-251. https://doi.org/10.1016/j.memsci.2008.10.007.
[57] M. Shakaib, S. Hasani, M. Mahmood, CFD modeling for flow and mass transfer in spacer-obstructed membrane feed channels, J. Membr. Sci. 326(2) (2009) 270-284. https://doi.org/10.1016/j.memsci.2008.09.052.
[58] C. Niu, X. Li, R. Dai, Z. Wang, Artificial intelligence-incorporated membrane fouling prediction for membrane-based processes in the past 20 years: A critical review, Water Res. 216 (2022) 118299. https://doi.org/10.1016/j.watres.2022.118299.
[59] S.S. Madaeni, N.T. Hasankiadeh, A.R. Kurdian, A. Rahimpour, Modeling and optimization of membrane fabrication using artificial neural network and genetic algorithm, Sep. Purif. Technol. 76(1) (2010) 33-43. https://doi.org/10.1016/j.seppur.2010.09.017.
[60] M. Barello, D. Manca, R. Patel, I.M. Mujtaba, Neural network based correlation for estimating water permeability constant in RO desalination process under fouling, Desalination 345 (2014) 101-111. https://doi.org/10.1016/j.desal.2014.04.016.
[61] L. Zhao, T. Dai, Z. Qiao, P. Sun, J. Hao, Y. Yang, Application of artificial intelligence to wastewater treatment: A bibliometric analysis and systematic review of technology, economy, management, and wastewater reuse, Process Saf. Environ. Prot. 133 (2020) 169-182. https://doi.org/10.1016/j.psep.2019.11.014.
[62] J. Schmidhuber, Deep learning in neural networks: An overview, Neural Networks 61 (2015) 85-117. https://doi.org/10.1016/j.neunet.2014.09.003.
[63] L.F. Greenlee, D.F. Lawler, B.D. Freeman, B. Marrot, P. Moulin, Reverse osmosis desalination: water sources, technology, and today's challenges, Water Res. 43(9) (2009) 2317-2348. https://doi.org/10.1016/j.watres.2009.03.010.